Electronic Supplementary Material (ESI) for RSC Advances.

Discrimination of sibutramine and its analogues based on surface-enhanced Raman spectroscopy and chemometrics: toward rapid detection of synthetic anorexic drug in natural slimming product

Hui Mao [a,b] , Meihui Qi [a], Yujie Zhou [a] , Xiaoyan Huang [a] , Liying Zhang [a] , Yang Jin [a] , Yan Peng [a] , Shuhu Du [a,*]

[a] *School of Pharmacy, Nanjing Medical University, Nanjing, China 211166*

[b] *Nuclear Medicine Department, Nanjing General Hospital of Nanjing Military Command, Nanjing, China 210002*

This document provides more detailed information to the paper mentioned above.

* Corresponding author. Tel./Fax: +86 25 86868476.

E-mail address: shuhudu@njmu.edu.cn.

LC-MS analysis conditions[1]

The chromatographic separation of SIB or its two analogues was performed on a Zorbax C18 column (50 mm × 2.1 mm and 1.8μm particle size) maintained at 25 °C. Mobile Phase A was 2mM of ammonium formate in water with 0.05% formic acid). Mobile Phase B was 2mM of ammonium formate in methanol with 0.05% formic acid. Gradient elution was performed starting with 30% Mobile Phase B, increasing to 90% B at 7 min and holding for 2 min, then changing to 30% Mobile Phase B at 10 min. The flow rate was set at 0.3 mL min^{-1} and the runtime of the method was 12 min. The source parameters were set as follows: dry gas temperature = 200 ^{o}C, drying gas flow = 11 L min^{-1}, nebulizer pressure = 45 psi, sheath gas temperature = 350 ^{o}C, sheath gas flow = 11 L min^{-1}, capillary potential = 3500 V, nozzle voltage = 500V. The collision energies were optimized with standard reference. The spectra were obtained in the positive ion mode.

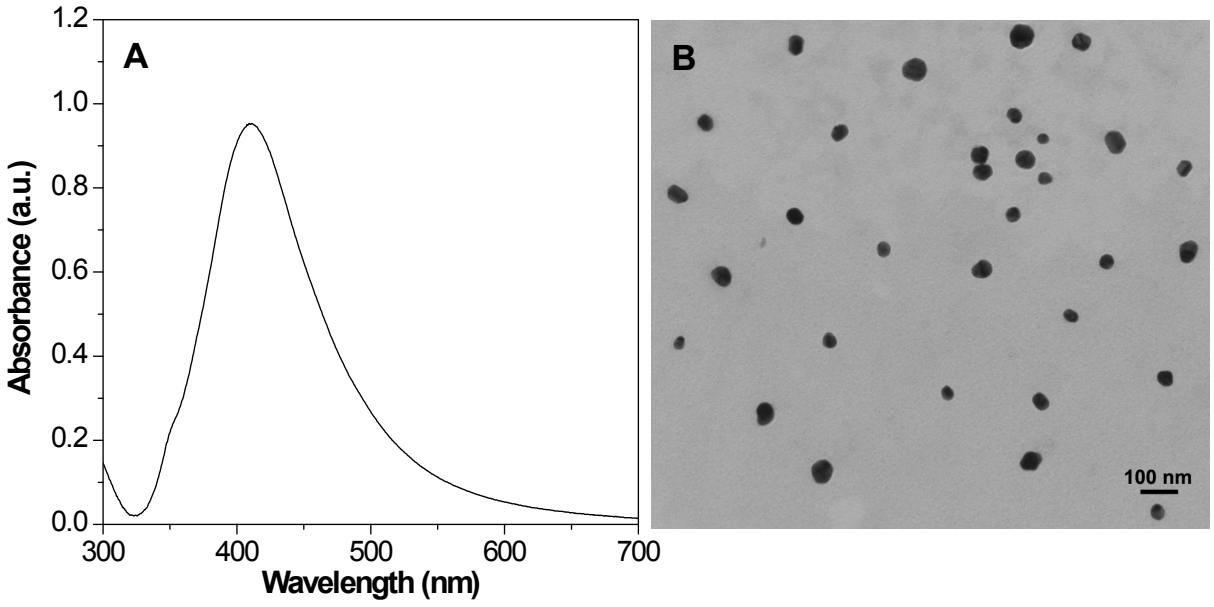

Fig. S1 (A) UV-vis absorption spectrum of Ag NPs colloid and (B) TEM image of Ag NPs.

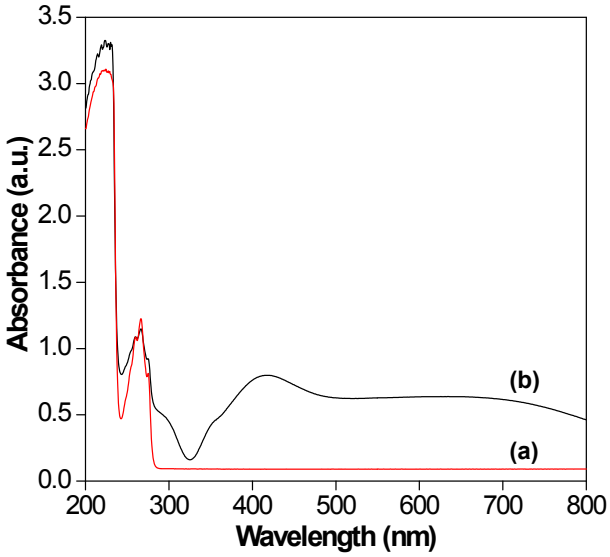

Fig. S2 UV-vis absorption spectra of (a) SIB and (b) SIB complexed with Ag NPs colloid.

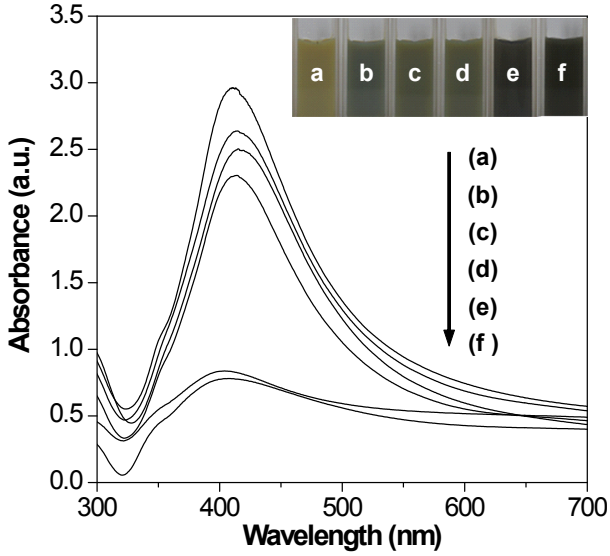

Fig. S3 UV-vis absorption spectrum of (a) pure Ag NPs colloid and the spectra when adding uniform concentration of (b) KI, (c) KNO_3, (d) KBr, (e) K_2CO_3 and (f) KCl, respectively (the inset shows the corresponding color images).

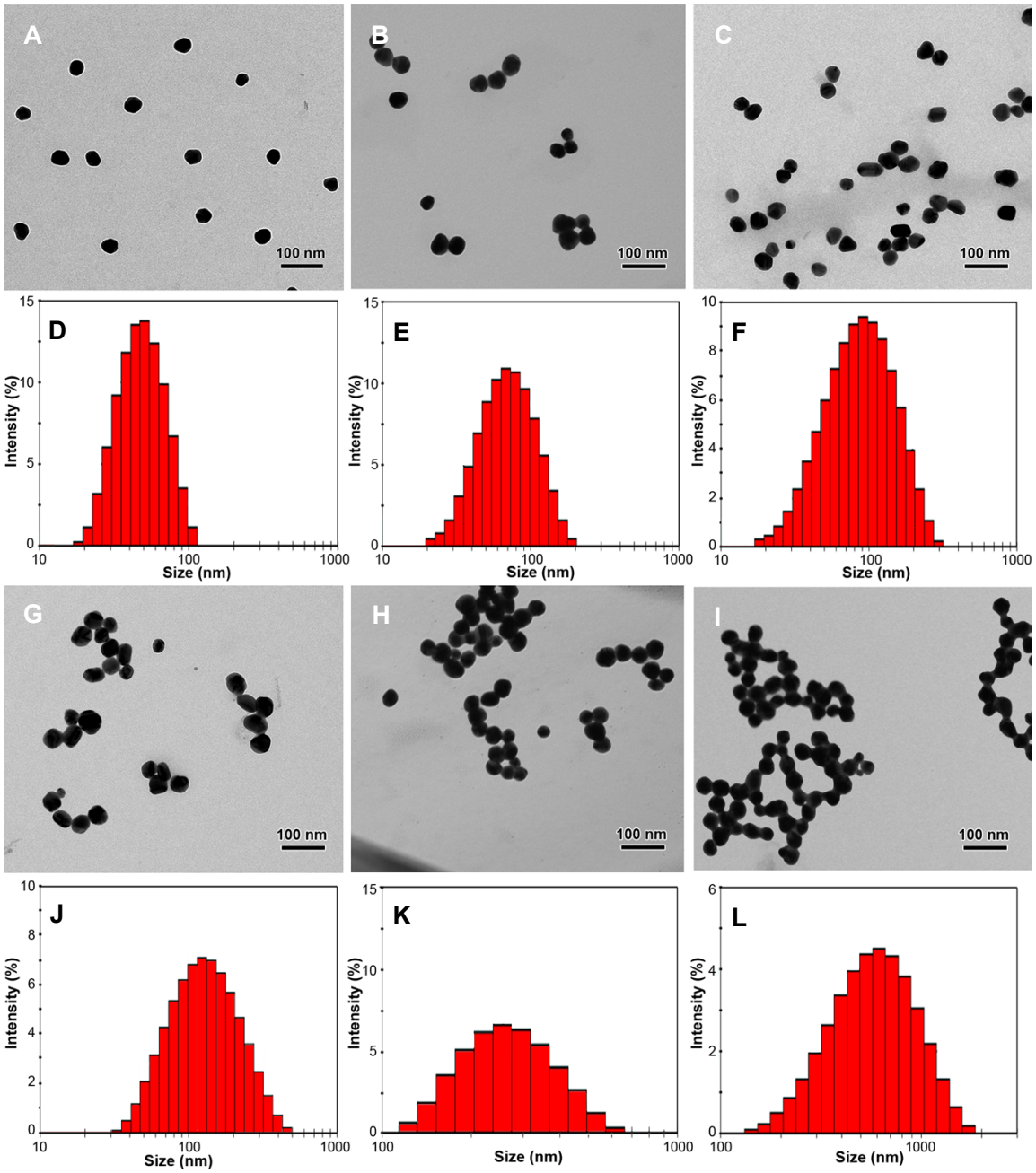

Fig. S4 TEM images of Ag NPs before (A) and after the addition of KI (B), KNO_3 (C), KBr (G), K_2CO_3 (H) and KCl (I). Size distribution histograms of Ag NPs before (D) and after the addition of KI (E), KNO_3 (F), KBr (J), K_2CO_3 (K) and KCl (L).

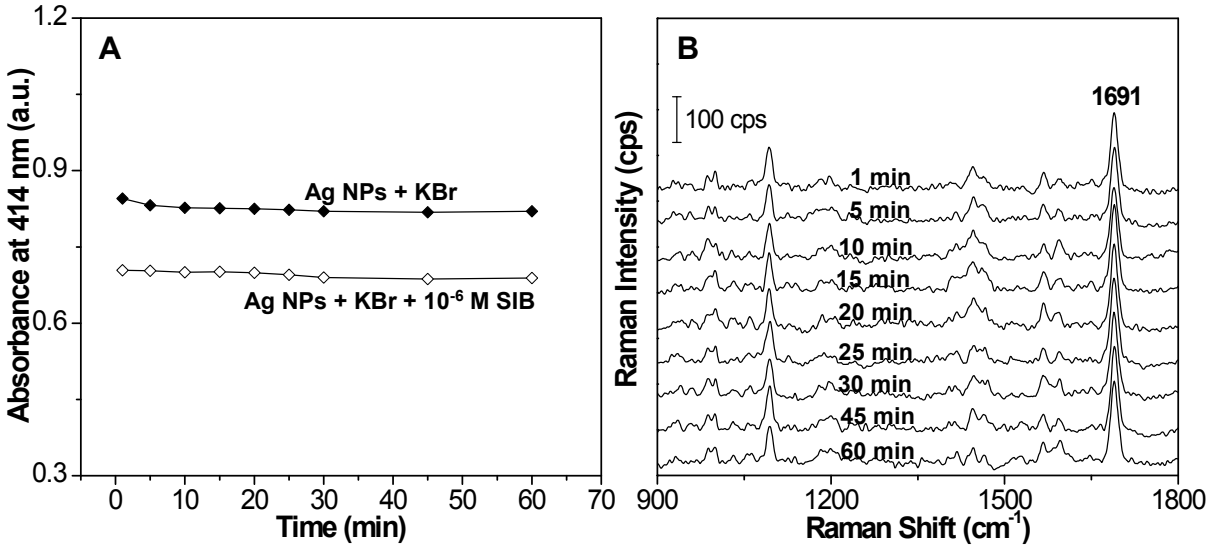

Fig. S5 (A) Evolutions of Ag NPs absorbance as a function of time after the addition of KBr and SIB. (B) SERS spectra of 1.00 × 10^{-6} M SIB absorbed on Ag NPs after the addition of KBr with the increase of time.

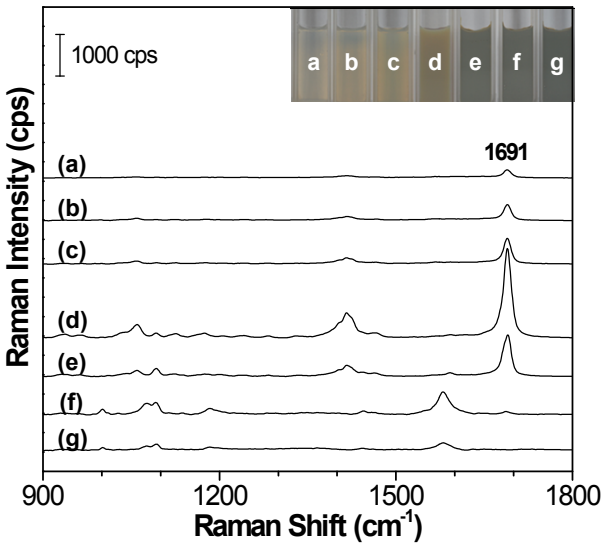

Fig. S6 Evolution of 5.00 × 10^{-5} M SIB Raman intensity (at 1691 cm^{-1}) with the different concentrations of Ag NPs colloid: (a) 0.007 nM, (b) 0.01 nM, (c) 0.02 nM, (d) 0.2 nM, (e) 2 nM, (f) 4 nM, and (g) 6 nM.

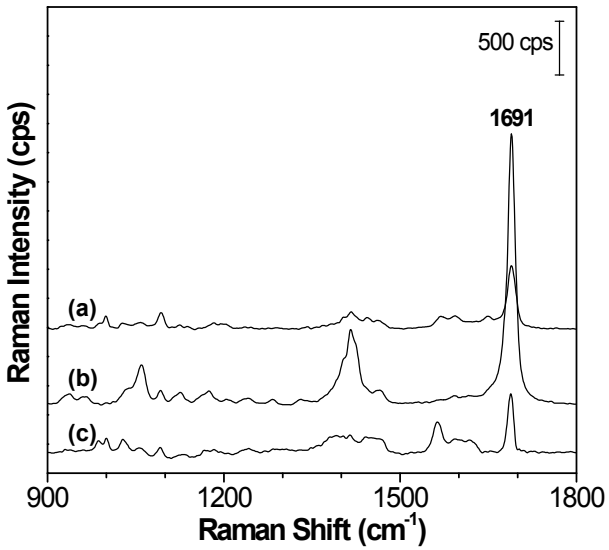

Fig. S7 Variation of 5.00×10^{-5} M SIB Raman intensity (at 1691 cm^{-1}) with different pH values: (a) 2.5, (b) 7.4 and (c) 11.5.

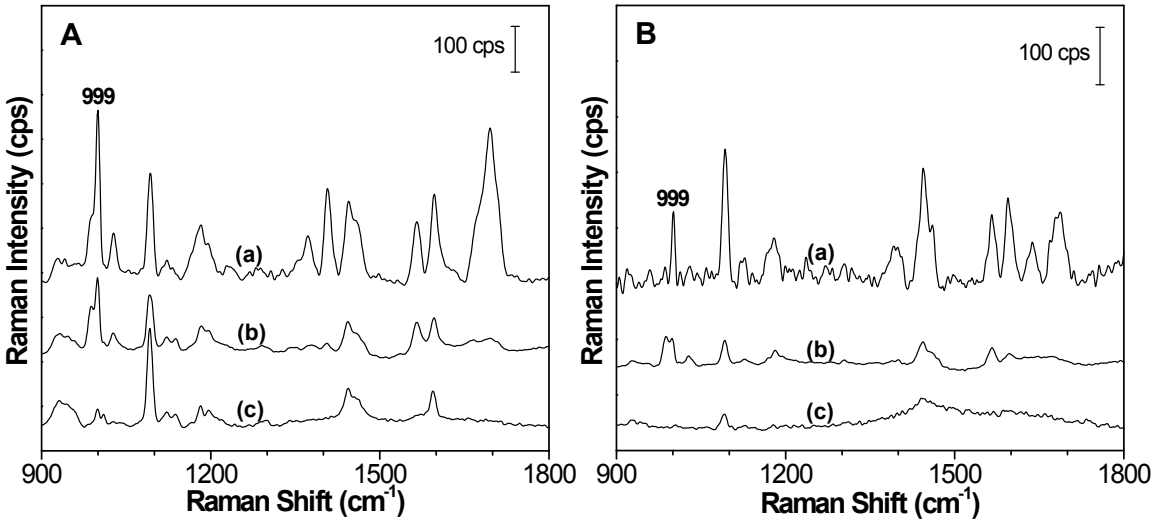

Fig. S8 SERS spectra of MDS (A) and DDS (B) absorbed on Ag NPs excited by different excitation wavelengths: (a) 532, (b) 633 and (c) 780 nm (the concentration of MDS and DDS is 5.00×10^{-5} M, respectively).

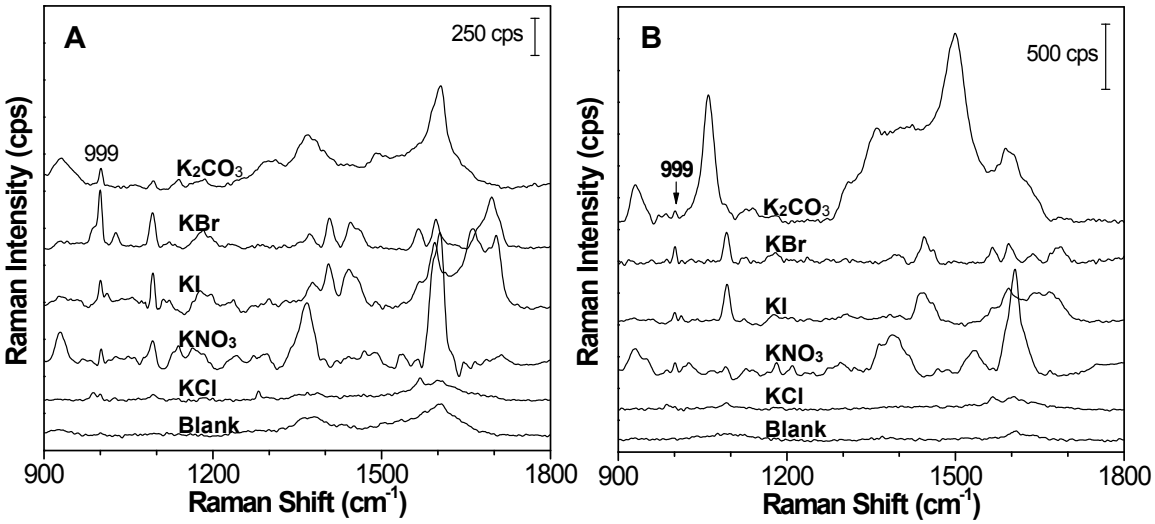

Fig. S9 Effects of aggregating agents on SERS intensity of MDS (A) and DDS (B) (the concentration of MDS and DDS is 5.00×10^{-5} M, respectively).

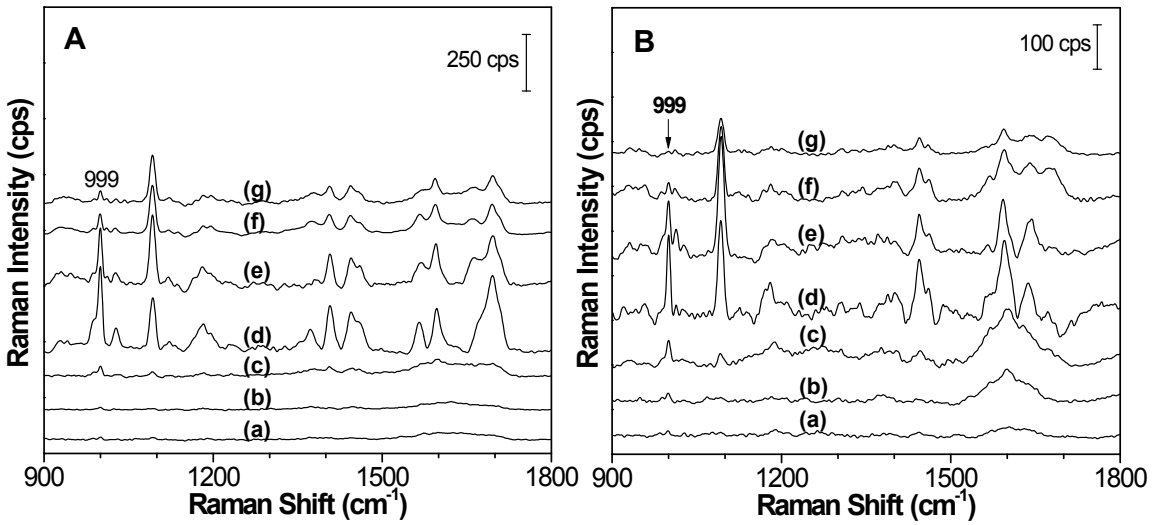

Fig. S10 Evolution of MDS (A) and DDS (B) Raman intensity (at 999 cm^{-1}) with the different concentrations of Ag NPs colloid: (a) 0.007 nM, (b) 0.01 nM, (c) 0.02 nM, (d) 0.2 nM, (e) 2 nM, (f) 4 nM, and (g) 6 nM (the concentration of MDS and DDS is 5.00×10^{-5} M and 1.00×10^{-4} M, respectively).

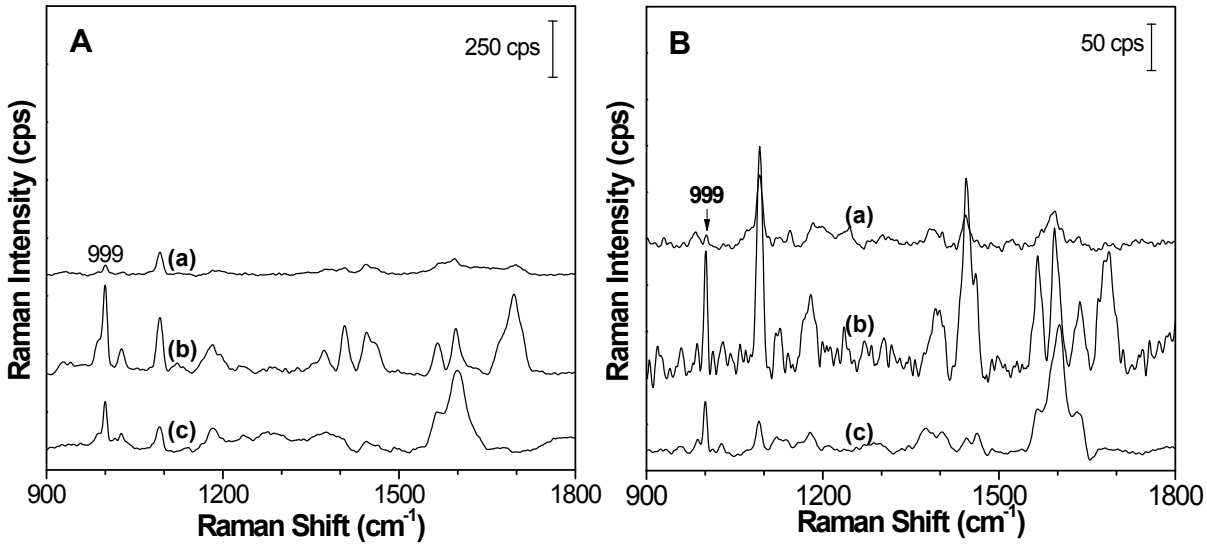

Fig. S11 Variation of MDS (A) and DDS (B) Raman intensity (at 999 cm^{-1}) with different pH values: (a) 2.5, (b) 7.4 and (c) 11.5 (the concentration of MDS and DDS is 5.00×10^{-5} M, respectively).

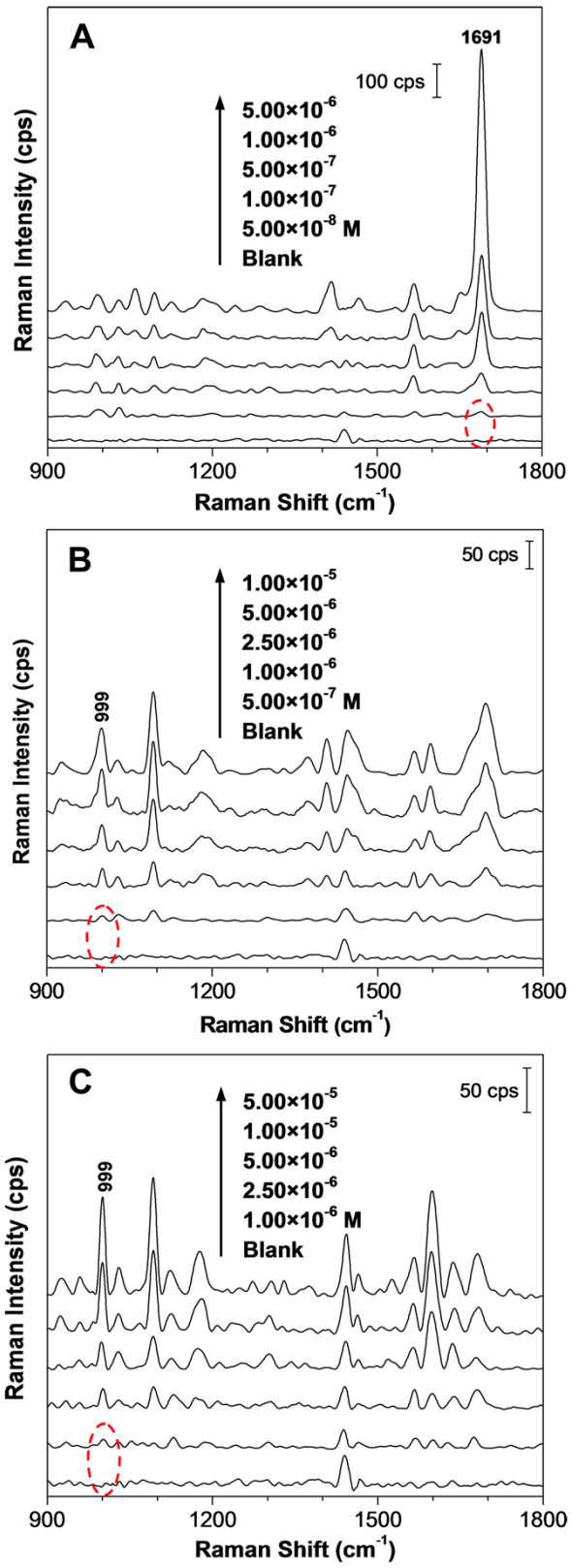

Fig. S12 SERS spectra of (A) SIB, (B) MDS and (C) DDS in Ag NPs colloid with increase of its amount, respectively.

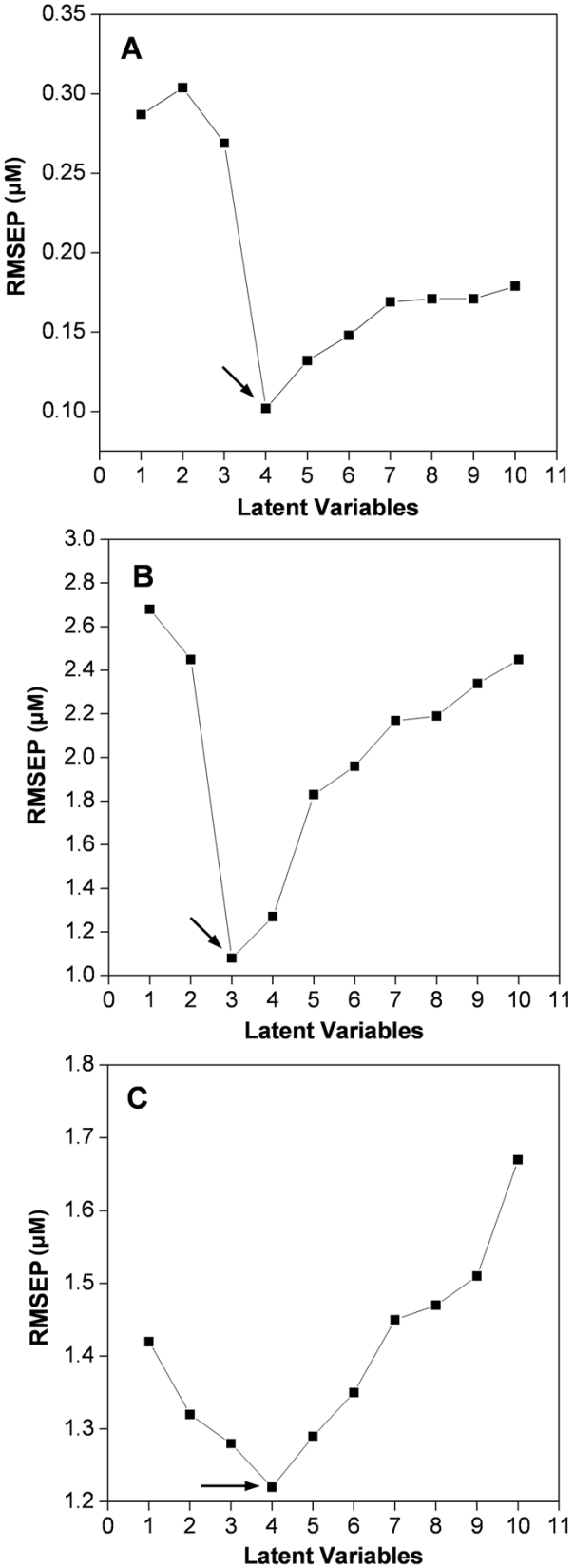

Fig. S13 RMSEP values obtained from PLS model based on (A) SIB, (B) MDS and (C) DDS spectra with different latent variables, respectively.

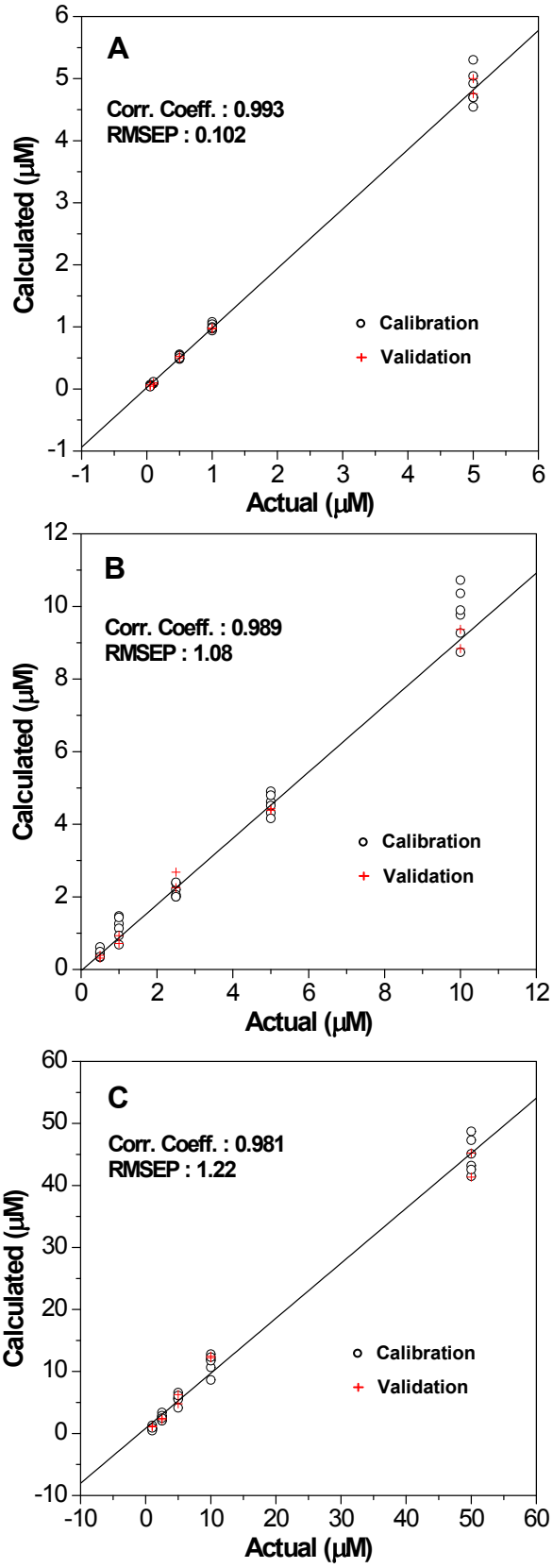

Fig. S14 Calibration curve for (A) SIB, (B) MDS and (C) DDS using the PLS models, respectively.

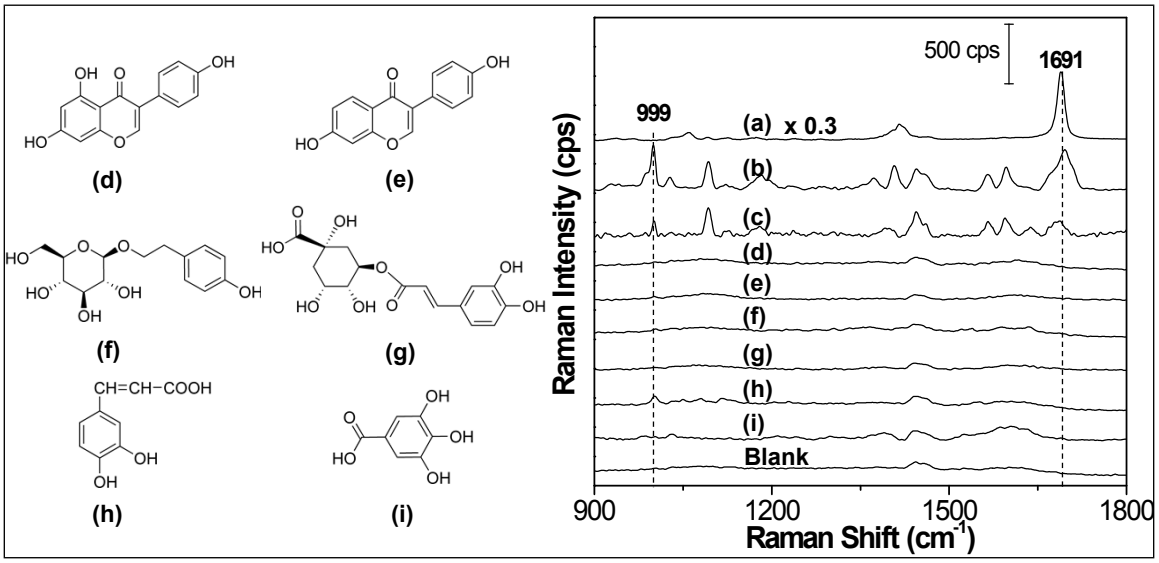

Fig. S15 Selectivity of Ag NPs for the detection of SIB, MDS, and DDS over other analogues. (a) SIB, (b) MDS, (c) DDS, (d) genistein, (e) daidzein, (f) salidroside, (g) chlorogenic acid, (h) caffeic acid and (i) gallic acid. The concentration of (a), (b) and (c) is 5.00×10^{-5} M, respectively. The concentration of (d), (e), (f), (g), (h) and (i) is 1.00×10^{-3} M, respectively.

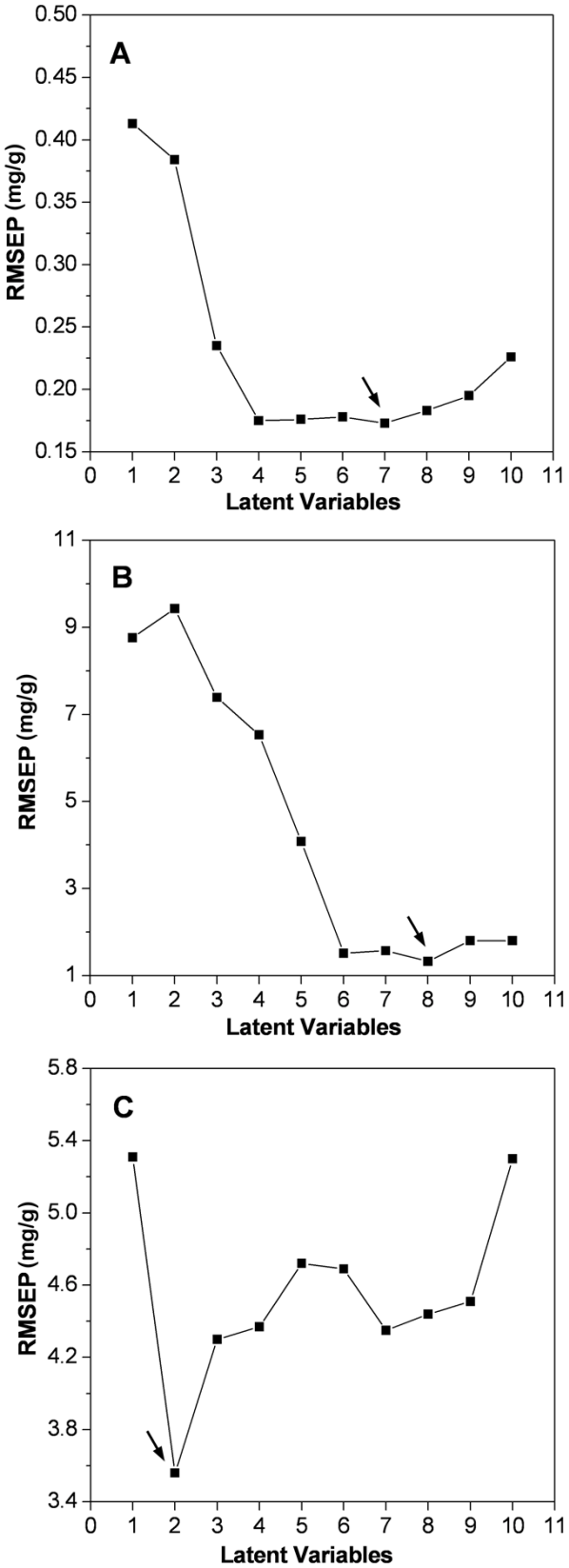

Fig. S16 RMSEP values obtained from PLS models based on (A) KPC with SIB, (B) KPC with MDS and (C) KPC with DDS spectra with different latent variables, respectively.

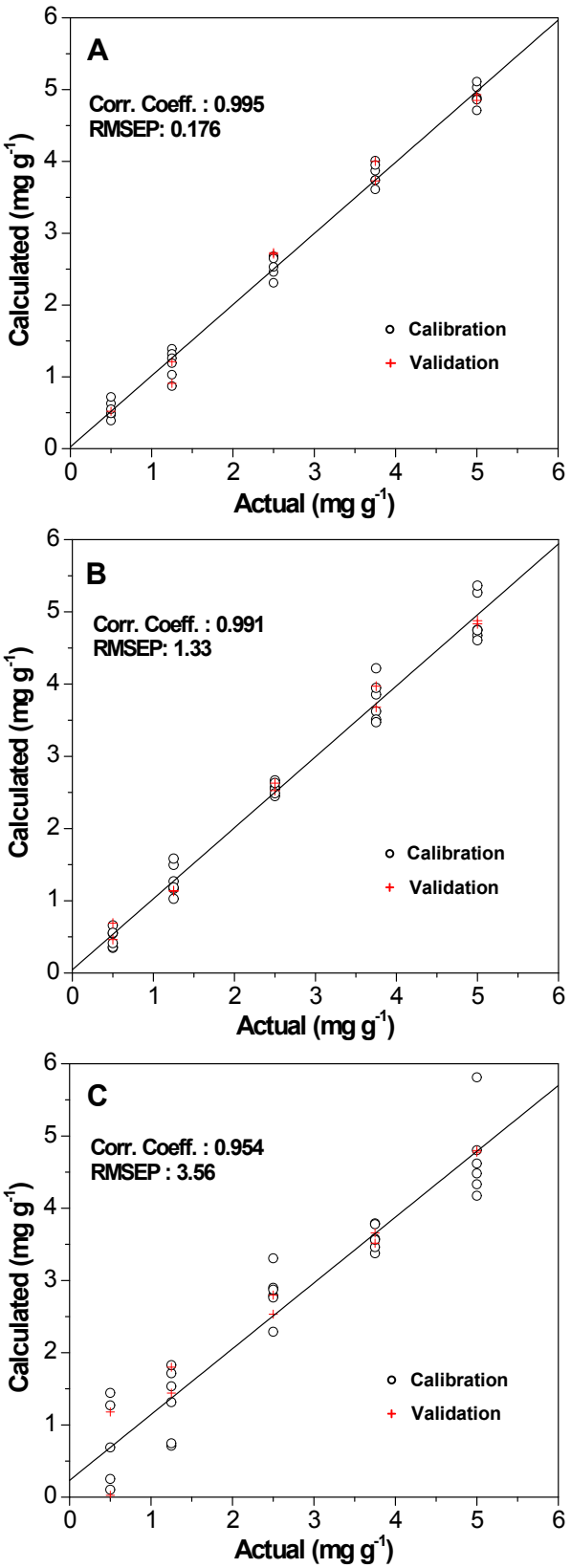

Fig. S17 Calibration curve for (A) SIB, (B) MDS and (C) DDS in KPC using the PLS models, respectively.

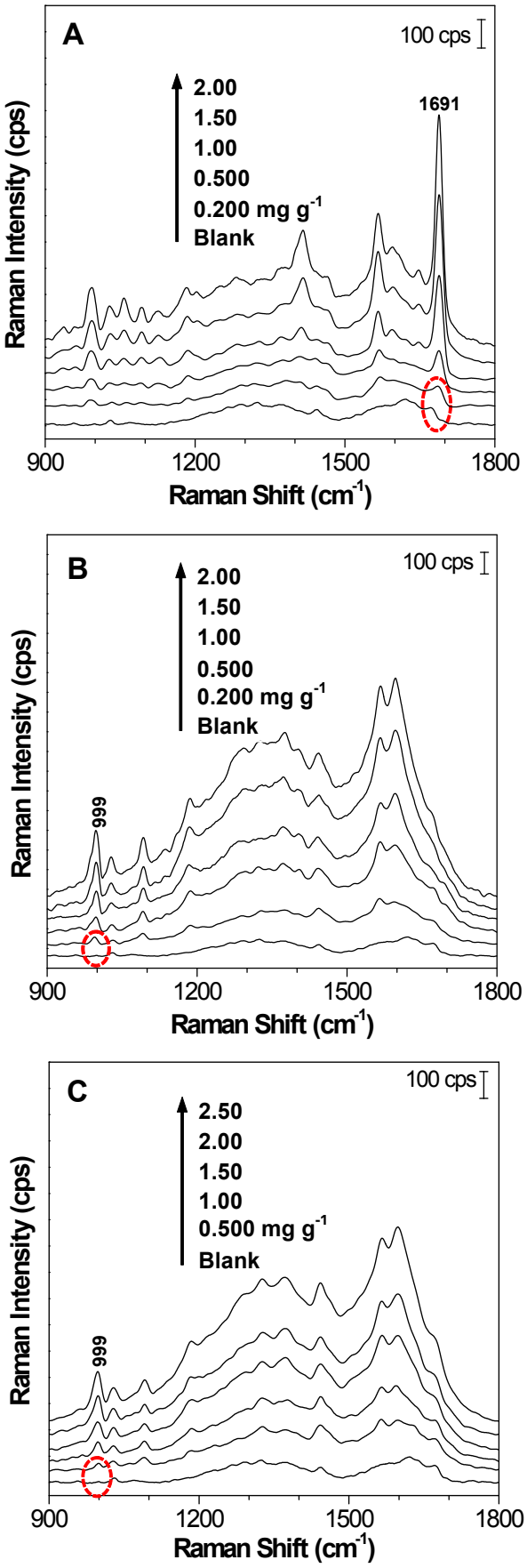

Fig. S18 SERS spectra of HST spiked with different amounts of (A) SIB, (B) MDS and (C)

DDS, respectively.

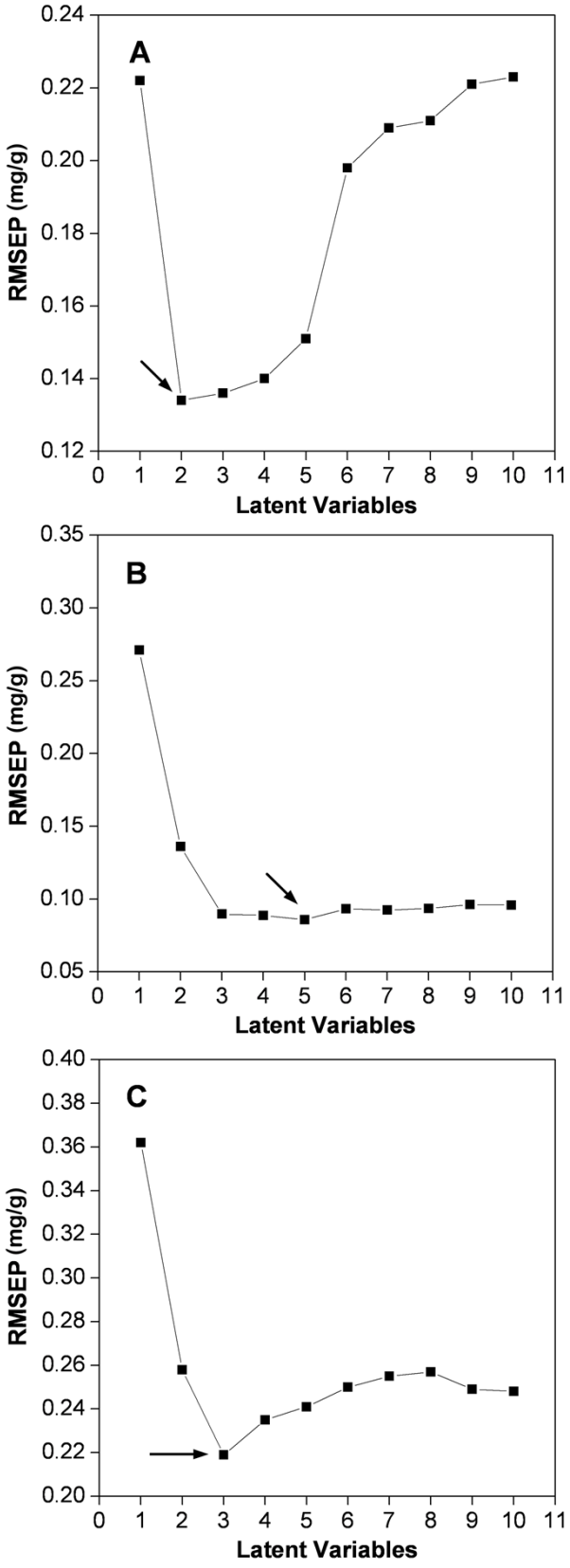

Fig. S19 RMSEP values obtained from PLS models based on (A) HST with SIB, (B) HST with MDS and (C) HST with DDS spectra with different latent variables, respectively.

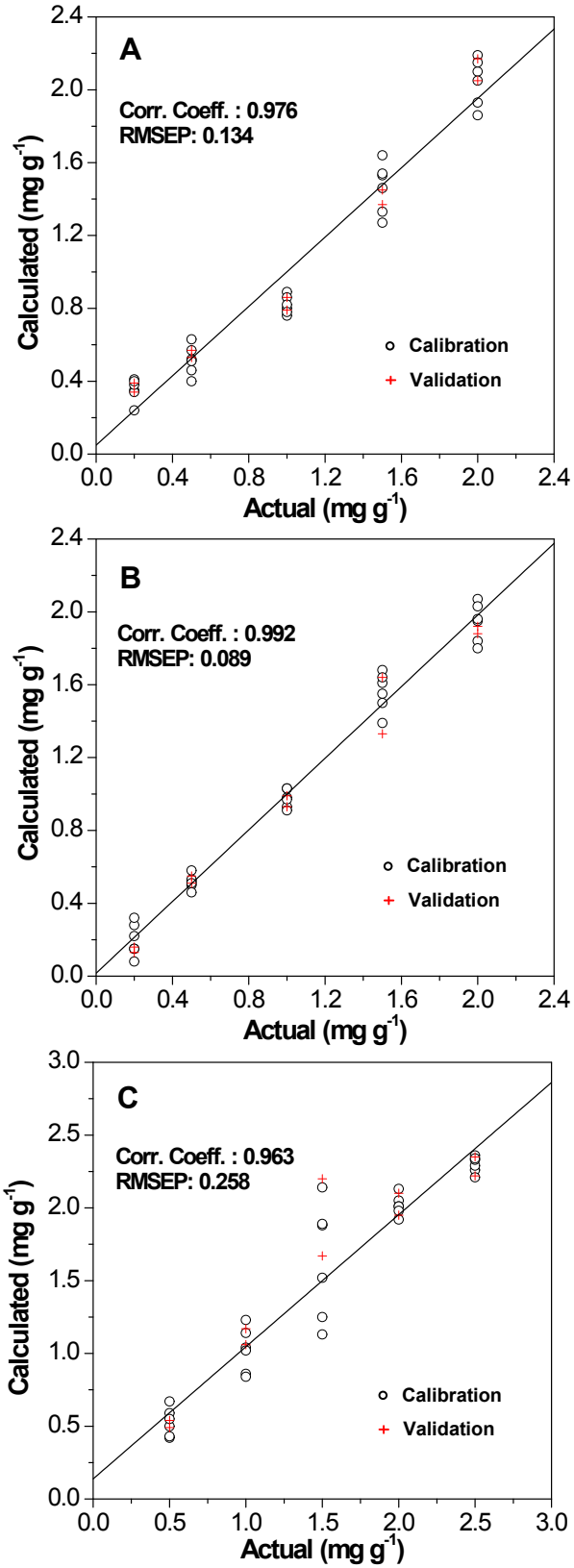

Fig. S20 Calibration curve for (A) SIB, (B) MDS and (C) DDS in HST using the PLS models, respectively.

Table S1 Real detections and recovery tests of SIB, MDS and DDS spiked in HST, respectively (n=6).

Sample	Spiked concentration (mg g^{-1})	Detected concentration (mg g^{-1})		Recovery (%)			
		Raman method	LC-MS method	Raman method	RSD (%)	LC-MS method	RSD (%)
SIB	0	nd*	nd*	-	-	-	-
	0.500	0.483	0.494	96.7	4.82	98.8	4.96
	1.00	0.985	0.992	98.5	4.21	99.2	4.33
	1.50	1.46	1.54	97.3	3.89	103	3.66
MDS	0	nd*	nd*	-	-	-	-
	0.500	0.502	0.489	100	5.03	97.8	4.74
	1.00	0.976	0.988	97.6	3.69	98.8	3.02
	1.50	1.45	1.48	96.7	2.40	98.7	2.78
DDS	0	nd*	nd*	-	-	-	-
	0.500	0.503	0.496	101	4.72	99.2	4.11
	1.00	0.983	0.979	98.3	3.29	97.9	3.50
	1.50	1.49	1.47	99.4	2.11	98.0	2.02

* Not detected.

References

1 F. H. Song, D. Monroe, A. El-Demerdash, C. Palmer, *J. Pharm. Biomed. Anal.*, 2014, **88**, 136−143.